Pakistan Veterinary Journal

ISSN: 0253-8318 (PRINT), 2074-7764 (ONLINE)
DOI: 10.29261/pakvetj/2025.271

RESEARCH ARTICLE

Effect of PI3K/AKT Pathway Modulation Mediated by Oncostatin M (OSM) on the Proliferation, Migration, and Extracellular Matrix Gene Expression of Donkey Skin Fibroblasts

Lei Liu [1†], Chunhao Zhu[1†], Yukun Zhao[1], Ronghua Shi[1], Hong Tao[1], Chenlong Wang[1], Tingting Zhu[1], Mingyang Geng[2], Weibin Zeng[1*] and Yanping Wang [1*]

[1] College of Animal Science and Technology, Shihezi University, Shihezi 832000, PR China; [2] Animal Husbandry Station, Ili Kazakh Autonomous Prefecture, Ili 835000, PR China.
*Corresponding author: zwbdky@126.com(WZ); wypdky@126.com(YW)

ARTICLE HISTORY (25-025)

Received: January 09, 2025
Revised: August 30, 2025
Accepted: September 04, 2025
Published online: October 13, 2025

Key words:
Donkey skin
Fibroblasts
OSM
PI3K/AKT pathway

A B S T R A C T

Donkeys exhibit a faster healing rate of dorsal skin wounds compared to their closely related counterparts, horses. This accelerated healing is accompanied by adequate collagen production without pathological over-deposition. However, studies exploring the underlying mechanisms of this superior wound healing in donkeys remain scarce. To explore the effects of OSM on the proliferation, migration, and extracellular matrix (ECM) gene expression of donkey skin fibroblasts, primary donkey skin fibroblasts were cultured and divided into four groups: OE-OSM, OE-NC, sh-OSM-2, and sh-NC. Cell viability was assessed using the Cell Counting Kit-8 (CCK-8) assay, and migration was evaluated through wound healing assays. Protein expression levels of collagen I (COL1), collagen III (COL3), and related factors were determined by Western blot (WB) analysis. Gene expression changes of COL1A1, COL3A1, Fibronectin (FN), and AKT Serine/threonine kinase 1 (AKT1) were quantified using RT-qPCR. Results indicated that OSM overexpression significantly reduced the proliferation and migration of donkey skin fibroblasts ($P<0.01$), while gene silencing produced opposite effects. Furthermore, overexpression of OSM notably reduced the expression levels of COL1A1, COL3A1, FN, and AKT1 ($P<0.01$), while simultaneously increasing Caspase-3 levels ($P<0.01$). These results suggest that OSM overexpression inhibits collagen synthesis (COL1 and COL3), reduces fibroblast proliferation and migration, and inhibits the PI3K/AKT signaling pathway.

To Cite This Article: Liu L, Zhu C, Zhao Y, Shi R, Tao H, Wang C, Zhu T, Geng M, Zeng W and Wang Y 2025. Effect of PI3K/AKT pathway modulation mediated by oncostatin m (osm) on the proliferation, migration, and extracellular matrix gene expression of donkey skin fibroblasts. Pak Vet J. http://dx.doi.org/10.29261/pakvetj/2025.271

INTRODUCTION

Skin repair following injury occurs through a complex wound healing process that typically culminates in scar formation (Zhu *et al.*, 2020). Fibroblasts play a critical role in wound healing by migrating into the injured area and proliferating during the early phases of the repair process (Peña and Martin, 2024). The extracellular matrix (ECM), which is composed of various biomolecules including collagen, fibronectin, laminin, and proteoglycans, forms the basis of tissue structure (Tracy *et al.,* 2016; Johnson *et al.*, 2020). The main cell types responsible for the production of these ECM proteins are fibroblasts, occupying a critical position in structural support and new matrix deposition that is crucial during the processes of tissue repair and regeneration (Seaton *et al.,* 2015; Sood *et al.*, 2015; Gardeazabal and Izeta, 2024). The collagen content in donkey skin is significantly higher than that in other animal tissues (Polidori *et al.*, 2020), and collagen cross-linking significantly promotes wound healing (Jørgensen *et al.*, 2020). Skin wounds in horses often develop into chronic wounds due to exercise-induced friction, a high infection risk, or delayed treatment, leading to excessive granulation tissue formation,a phenomenon rarely observed in donkeys (Iacopetti *et al.*, 2020). For the same reasons, distal limb wounds in equids are more difficult to heal than trunk wounds (Anantama *et al.*, 2022).

Oncostatin M (OSM) is a member of the interleukin 6 (IL-6) family of cytokines, whose pleiotropic effectors mediate its activity through the activation of multiple signaling pathways, including the MAPK and PI3K/AKT pathway (Han *et al.*, 2021; Caligiuri *et al.*, 2022; Polak *et*

al., 2023). OSM controls the breakdown and repair of the ECM by balancing enzymes (Matrix Metalloproteinases, MMPs) and their inhibitors (Tissue Inhibitors of Metalloproteinases, TIMPs) (Richards, 2013). Therefore, OSM can regulate the synthesis and degradation of collagen. In chronic rhinosinusitis with nasal polyps (CRSwNP), OSM has been shown to block transforming growth factor-β (TGF-β) from increasing alpha smooth muscle actin (α-SMA) and inhibits collagen and fibronectin production (Carsuzaa *et al.*, 2022). In kidney models, OSM reduces collagen I/III and fibronectin by blocking TGF-β activation of SMAD proteins (Mashimo *et al.*, 2021). However, studies have demonstrated fewer OSM-positive cells in human heart fibrosis areas (Abe *et al*., 2019). These findings reveal tissue specificity across different organs. Beyond inflammation and scarring, OSM influences cell proliferation, migration, and differentiation (Wei *et al.*, 2023). Although OSM exerts distinct effects on cellular behavior and ECM remodeling across different tissues, its effects on equine skin fibroblasts remain poorly defined and require further investigation.

The Akt pathway, also termed the protein kinase B (PKB) pathway, represents an important node in cellular signaling that, very broadly, regulates growth, proliferation (Hao *et al.*, 2023), glucose metabolism, cell migration (Graupera *et al.*, 2008), and angiogenesis. PI3K/Akt pathway inhibition, by BUB1 protein knockdown, resulted in the inhibition of proliferation and migration in rheumatoid arthritis synovial fibroblast cells (MH7A) (He *et al.,* 2023). This pathway further showed considerable indication of fibroblast activation and production of collagen (He *et al.*, 2023). During skin fibrosis, the FAK/PI3K/AKT and TGF-β signaling pathways were shown to synergistically drive fibroblast activation and collagen deposition (Huang *et al.*, 2023). The presented expression of regulatory effects of the Akt pathway in donkey skin fibroblasts helps to establish their biological response during skin injury repair and atrophy.

Although the skin healing properties of equids have been investigated (Azari *et al.*, 2012), the association between OSM signaling pathways, particularly the PI3K/AKT pathway, and ECM regulation in donkey skin fibroblasts remains entirely unaddressed. The structural features of donkey skin, including dense collagen fiber bundles and sparse glands (Mohammed *et al.*, 2022), may endow its OSM signaling response with distinct characteristics compared to other species. While the PI3K/AKT pathway is central to fibroblast activation and collagen deposition (Huang *et al.*, 2023; He *et al.*, 2024), whether OSM regulates the proliferation and migration of donkey fibroblasts and mediates collagen metabolism through this pathway has not been directly validated. This mechanistic gap hinders our understanding of the molecular basis for efficient wound healing in donkey skin (Knottenbelt, 2019). Based on the PI3K/AKT pathway as the most relevant signaling axis, we hypothesize that OSM promotes early-stage wound healing in donkey skin fibroblasts by activating the PI3K/AKT pathway. This activation synergistically regulates fibroblast proliferation, migration, and the balance between ECM synthesis and degradation.

Thus, in this study conducted on donkey skin fibroblasts *in vitro*, OSM overexpression and interference vectors were constructed to investigate their impact on gene expression related to fibroblast proliferation, migration, and fibrosis. Additionally, the influence of OSM on the healing of donkey skin wounds via the PI3K/AKT pathway was examined, aiming to provide theoretical evidence for understanding the mechanisms of skin wound healing and the potential treatment of fibrotic diseases in later healing stages.

MATERIALS AND METHODS

Plasmid construction: OSM overexpression (OE-OSM) vectors, OSM knockdown vectors (three small interfering RNAs (siRNAs)), and their respective controls (siRNA-NC) were synthesized by GenePharma (Shanghai, China) (Table 1). The plasmid backbone (pGPU6/GFP/Neo, Cat#C02007) was double digested with BbsI and BamHI restriction enzymes. The target gene fragment was inserted into the digested backbone via T4 DNA ligase-mediated ligation, followed by transformation into *E. coli* DH5α competent cells. Positive clones were screened by colony PCR using gene-specific primers and further verified by Sanger sequencing to confirm the correct insertion and orientation of the target gene.

Table 1: RNA interference target sequences

siRNA	Sequences (5′-3′)
sh-OSM-1	F:CTGGCTAACGGGTGACAATGAA
	R:TTCATTGTCACCGTTAGCCAG
sh-OSM-2	F:CACCTCTCAGAAGCACTTTAA
	R:TTAAAGTGCTTCTGAGAGGTG
sh-OSM-3	F:AGGGGCCAACTTTCCATTGAT
	R:ATCAATGGAAAGTTGGCCCCT

Lentiviral packaging: The target gene plasmid was co-transfected with pSPAX2 and pMD2G into 293T cells at a mass ratio of 4:3:1. After 48 hours, the supernatant was collected, filtered, and transferred to a Millipore Amicon Ultra-15 Centrifugal Filter Unit (Cat#UFC905008, Merck, Germany), and concentrated by centrifugation at 5,000g for 5 minutes. Prior to lentiviral transfection, Opti-MEM (Cat# 31985062, Invitrogen, USA) was used, along with an adequate volume of viral supernatant and 5mg/mL polybrene (Cat# H8761, Solebo, China). Following lentiviral packaging, the virus was diluted from 10^{-1} to 10^{-9} using the gradient dilution method. 100μL of the virus solution was added per well, with each dilution replicated three times. After 24 hours, the medium was replaced with fresh medium. The viral integration was evaluated after 96 hours by observing the fluorescence expression of the cells, and the viral titer was calculated using the formula:

Viral titer = number of fluorescent cells × dilution × 1000

Cell transfection: Fibroblasts were isolated from the dorsal skin tissue of Xinjiang donkeys using the tissue explant attachment method for primary culture. The cells were purified by trypsin digestion combined with the differential attachment method. Third-passage fibroblasts exhibiting the highest viability were selected for subsequent experiments (Zhu *et al.*, 2023). Primary donkey skin fibroblasts were seeded into 6-well plates at a density of 1×10^6 cells per well, with three replicates per experimental group (n=3). Cells were cultured in 2 mL of

complete DMEM medium (Cat#11965118, Gibco, Grand Island, NE, USA) for 10 hours at 37°C in a humidified incubator with 5% CO_2. Upon reaching 70–80% confluence, the medium was removed, and cells were rinsed twice using 1 mL of pre-chilled PBS. The experimental groups were designated as follows: OE-OSM group, OE-OSM negative control (OE-OSM-NC) group, sh-OSM group, and sh-OSM negative control (sh-OSM-NC) group. In the OE-OSM group, fibroblasts were transfected at an MOI of 30 with lentivirus containing the OSM-overexpressing construct. An empty vector lentivirus served as a control (OE-OSM-NC). In the sh-OSM group, fibroblasts were transfected using lentiviral shRNA vectors targeting OSM; the shRNA sequence with the highest efficiency, identified during prior screening, was selected. A non-targeting shRNA construct served as the negative control (sh-OSM-NC). Transfections for all groups were performed using Lipofectamine 3000 (Invitrogen, USA). Four hours after transfection, the culture medium was supplemented with half the original volume of fresh medium. Cells were subsequently cultured for an additional 48 hours before harvesting for downstream analyses.

CCK-8 assay: Transfected cells were seeded at a density of 2,000 cells per well into 96-well plates and cultured overnight. Each well was supplemented with 10μL of CCK-8 solution (Dojindo, Japan), and the incubation process persisted for approximately 2.5 hours. Optical density (OD) was measured at 450nm using a microplate reader (Multiskan SkyHigh, Thermo Fisher Scientific, USA). For each sample, triplicate technical replicates were averaged. Growth curves were plotted using time as the horizontal axis and OD values as the vertical axis, with measurements taken at 24, 36, 48, 60-, 72-, 84-, and 96-hours post-seeding (six replicates per time point).

Scratch experiment: A six-well plate was prepared by drawing three horizontal lines (n=3) across the bottom of each well using a marker and a straightedge. After being transfected with shRNA or infiltrated with viruses, third-generation skin fibroblasts from donkeys were trypsinized and resuspended, then adjusted to a concentration of 5×10^5 cells per well. Using a crisscross shaking procedure, the cells were spread equally. Using a 10μL pipette tip, a straight scratch was made at 90% confluence. After removing the excess culture medium and washing with PBS, complete DMEM medium containing 10% fetal bovine serum (FBS) was added for subsequent incubation. Using an inverted microscope, three fields of view were captured at 0, 36, and 72 hours to document the scratches (n=3).

Clone formation assay: For uniform distribution, stably transfected donkey skin fibroblasts were trypsinized, counted, and seeded into six-well plates at a density of 100 cells per well. To ensure the reliability of the experimental results, the experiment was repeated three times. Individual adherent cells were cultured *in vitro* for approximately two to three weeks, allowing them to proliferate beyond six generations and form colonies containing more than 50 cells. After 30 minutes of fixation in 4% paraformaldehyde, the cells were rinsed with PBS. Crystal violet was then added for 10 minutes, followed by rinsing under running water. Finally, photographs were taken.

RT-qPCR: After collecting granulocytes 48 hours after transfection, the Tiangen Tissue/Cell RNA Extraction Kit (Cat#DP419) was used to recover total RNA. An equal volume of chloroform was added, followed by vortex mixing and centrifugation at 12,000g for 15 minutes. The upper aqueous phase was carefully transferred to a new tube, to which 1.5 volumes of absolute ethanol were added and mixed thoroughly. This mixture was transferred into a spin column and centrifuged at 12,000g for 1 minute, and the flow-through was discarded. The column was washed with Buffer RW1 and centrifuged at 12,000g for 1 minute, discarding the flow-through afterward. Subsequently, Buffer RW2 (previously diluted with absolute ethanol) was added to the spin column, centrifuged at 12,000g for 2 minutes, and the flow-through was discarded. To remove residual ethanol, the empty spin column was centrifuged again at 12,000g for 1 minute. The spin column was then placed in a fresh collection tube, and RNA was eluted by adding 30–50μL of pre-warmed (65°C) RNase-free water. After incubating at room temperature for 2 minutes, the column was centrifuged at 12,000g for 2 minutes to collect the purified Total RNA was reverse-transcribed into cDNA using the PrimeScript RT Master Mix (Perfect Real Time) Kit (Cat#RR036A, TaKaRa , Japan) according to the manufacturer's protocol. The reaction system (20μL) contained 4μL of 5× PrimeScript Buffer for Real Time, 1μL of PrimeScript RT Enzyme Mix I, 1μL of Oligo dT Primer (50μM), 1μL of Random 6 mers (100μM), 1μg of total RNA, and RNase-free water to make up the volume. The reaction conditions were; incubation at 37°C for 15 minutes (reverse transcription), treatment at 85°C for 5 seconds (enzyme inactivation), followed by storage at 4°C. Before qPCR analysis, the cDNA was diluted 1:5 with nuclease-free water. Real-time quantitative PCR was performed using a LightCycler 96 Real-Time PCR System (Roche Diagnostics, Switzerland). The following ingredients were used in a 20μL reaction volume: 10μL of SYBR Green qPCR mix, 2μL of 50ng/μL cDNA, 6.4μL of ddH_2O, and 1.6μL of 10μmol/μL primers, all of which served as the template for the RT-qPCR. The temperature cycling protocol included a 5-second warmup at 95°C, 40 cycles of 5-second warmups at 95°C, and 30-second cooldowns. The relative mRNA expression was determined using the $2^{-\Delta\Delta CT}$ method, with three replicates per group, with donkey GAPDH serving as the internal control. All primers were designed by the research team and produced by Sangon Biotech (Shanghai, China) (Table 2).

Screening of effective concentrations of PI3K agonist (740Y-P) and inhibitor (PI-103): To develop a drug-treated donkey skin fibroblast model, a concentration gradient was established for 740Y-P at 0, 1, 5, 10, 20, and 30μmol/L, and for PI-103 at 0, 0.1, 0.5, 1, 2.5, 5, and 10μmol/L. 96-well plates were used to seed fourth-generation donkey skin fibroblasts at a density of 1×10^4 cells/mL per well. After 100μL of cell suspension was added to each well and left to incubate overnight, the medium was changed to include different doses of drugs. After 48 hours of co-cultivation, the CCK-8 reagent was added. For each concentration, the mean value was calculated using three replicates.

Western Blot (WB): Proteins were extracted using RIPA (Cat#89900, Invitrogen, USA) and 1% protease inhibitor

Table 2: PCR primer sequences used for quantitative gene expression analysis.

genetics	Primer sequence (5'-3')	Annealing temperature/°C	NCBI Serial Number
OSM	F: TGCACAGGTTGACCGCTTTACAG R: AGGCAGTGGGATGTTGTTCTGGAAC	62	XM_014834926.2
COL1A1	F: CTGAGCCAGCAGATCGAGAACATC R: TCCAGTATTCTCCGCTCTTCCAGTC	61	NM_001323779.1
COL3A1	F: TGGTTACTGCTTGCTCTGCTTCATC R: CACAGACGCATATTTGGCATGGTTC	61	XM_014852914.2
AKT1	F: TCAAGAGGCAGGAGGAAGAGATGG R: TTCATGGTCACACGGTGTTTGGGG	63	XM_044774409.1
Caspase-3	F:ACATGGAAGCAAGTCAATGGAC R: ACCAGGTGCTGTGGAATACG	61	XM_044760560.1
FN	F: GTGCTATTTGCTCCTGCACA R: GGCAGTTGACATTGGTGTTG	61	XM_014843578.2
GAPDH	F:CGACATCCGTAAGGACCTGT R: CAGGGGCTGTGATCTCCTTCT	61	XM_044756267.1

(Cat#I3911, Roche, Switzerland). The protein concentration was determined by plotting a curve according to the BCA protein concentration determination kit (Cat#PC0020, Solarbio, China). SDS loading buffer (5×) (Cat#P0015L, Beyotime, China) was added in a 1:4 ratio. Before being stored at -80°C, the samples were mixed completely and then heated in a water bath at 100°C for 5 minutes. A 10% SDS-PAGE gel was electrophoresed at 80V for 20 minutes and 120V for 60 minutes after 30 micrograms of denatured protein were put onto the gel. Activated PVDF membranes (Cat#IPVH00010, Merck Millipore, Germany) were used to transfer proteins after electrophoresis for 90 minutes at 150mA. Prior to incubation with primary antibodies against AKT, phosphorylated AKT, COL1, COL3, and GAPDH, the membranes were blocked at room temperature for 2 hours, followed by three 10-minute washing with TBST. Overnight at 4°C, the incubation continued. After three washes with TBST the next day, the membranes were incubated with fluorescent secondary antibodies for one hour, followed by another wash, and finally, visualization via autofluorescence imaging using a Bio-Rad GelDoc EZ Imager (Hercules, CA, USA). Three replicates were used for each group to quantify band intensity using ImageJ software. Relative expression of target proteins was then determined by normalizing to GAPDH. Table 3 lists the antibodies that were employed.

Table 3: Antibodies and their dilutions used for WB analysis

Reagent Name	dilution ratio	provider	Lot number
Rabbit anti-COL1A1 poly antibody	1:1000	Beijing Bioss	bs-7158R
Rabbit anti-COL3A1 poly antibody	1:1000	Beijing Bioss	bs-0549R
Rabbit anti-p-AKT poly antibody	1:1000	Beijing Bioss	bs-0876R
Rabbit anti-AKT polyclonal antibody	1:1000	Beijing Bioss	bs-0115R
Rabbit anti-GAPDH polyclonal antibody	1:10,000	Wuhan Boster	A00227-1
Mouse Anti-Human IgG	1:2000	Beijing Bioss	bs-0297M

Statistical analysis: Statistical analyses were accomplished by GraphPad Prism 8.0 software. The normality of data was studied using the Shapiro-Wilk test, and all data were found to be normally distributed. Data are presented as the mean ± standard deviation (SD). Comparisons among multiple groups were conducted through one-way repeated measures ANOVA, and pairwise comparisons between groups were performed using the Least Significant Difference Test. Statistical significance was defined as *P<0.05 and **P<0.01

RESULTS

Effects of OSM overexpression and silencing on donkey skin fibroblasts: To elucidate the role of OSM in donkey skin fibroblasts, siRNA for OSM (si-OSM and si-OSM-NC) and overexpression vectors (OE-OSM and OE-OSM-NC) were packaged into lentiviruses in 293T cells and introduced into donkey skin fibroblasts. The impact of OSM manipulation on fibroblast proliferation and migration was assessed. RT-qPCR results (Fig. 1A) showed that OSM mRNA levels increased significantly (P<0.01) after overexpression compared to the control, confirming successful overexpression. The silencing efficiencies of sh-OSM-1, sh-OSM-2, and sh-OSM-3 were 35.41%, 65.95%, and 50.62%, respectively, with sh-OSM-2 being the most effective. Compared with the OE-OSM-NC group, the OE-OSM group exhibited significantly decreased cell proliferation rates, colony formation efficiency, and migration rates (P<0.01). Conversely, compared with the sh-OSM-NC group, the sh-OSM-2 group showed significantly increased cell proliferation rates, colony formation efficiency, and migration rates (P<0.01) (Fig. 1B-F).

OSM represses transcription of key ECN genes: The OE-OSM group exhibited significantly reduced mRNA expression of COL1A1, COL3A1, AKT1, and FN compared to the OE-NC group (P<0.01), whereas Caspase-3 mRNA expression was upregulated (P<0.01). Conversely, compared with the sh-NC group, the sh-OSM-2 group showed significantly upregulated mRNA expression levels of COL1A1, COL3A1, AKT1, and FN (P<0.01), while Caspase-3 mRNA expression was downregulated (P<0.01) (Fig. 2).

OSM inhibits collagen COL1 and COL3 expression: As critical components of the ECM, type I and III collagens significantly affect tissue fibrosis and scar formation. WB analysis (Fig. 3) demonstrated that compared with the OE-NC group, the OE-OSM group showed significantly downregulated protein levels of COL1 and COL3 (P<0.01). Conversely, the sh-OSM-2 group exhibited significantly upregulated COL1 and COL3 protein levels compared with the sh-NC group (P<0.01).

OSM inhibits the PI3K/AKT pathway in donkey skin fibroblasts: PI-103 showed a significant inhibitory effect on cells at concentrations above 1μmol/L (P<0.01); whereas 740Y-P enhanced cell proliferation significantly at 10μmol/L (P<0.01). To prevent cell inactivation from high

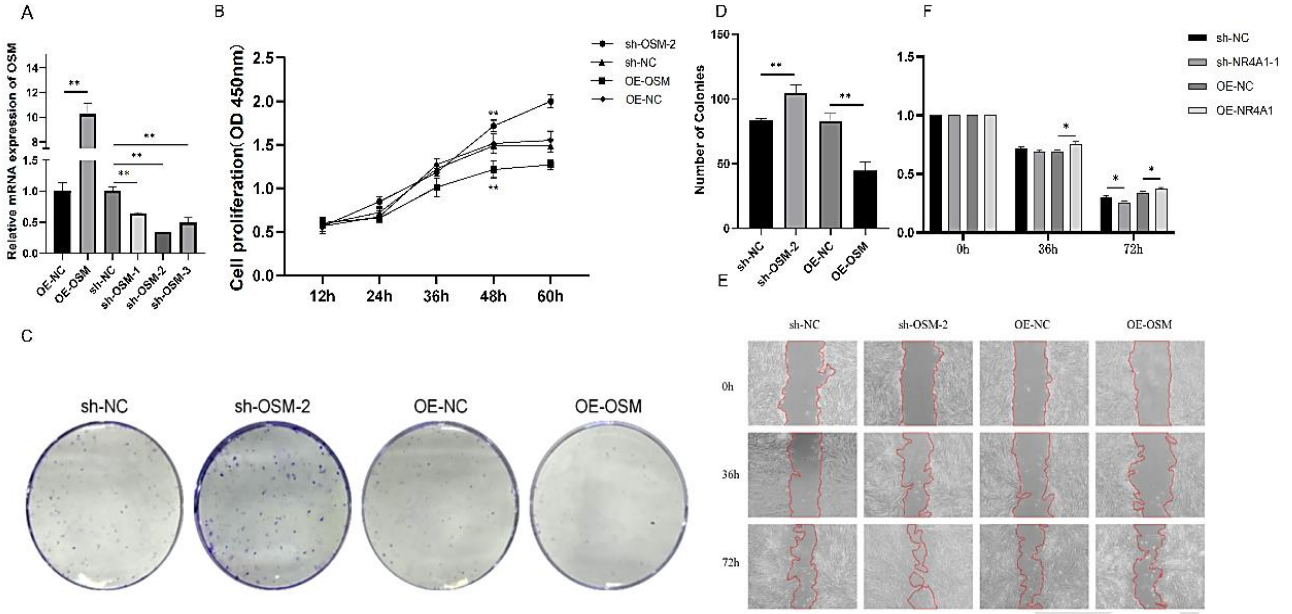

Fig. 1: Effects of Overexpression and Interference with OSM on Donkey Skin Fibroblasts; A:OSM Gene Expression; B: Cell Proliferation Curves; C: Colony Formation Assay; D: Cell Cluster Counting; E: Impact of OSM on Cell Migration; F: Scratch Area Ratio at Various Time Points.**P<0.01 n=3 biological replicates per condition.

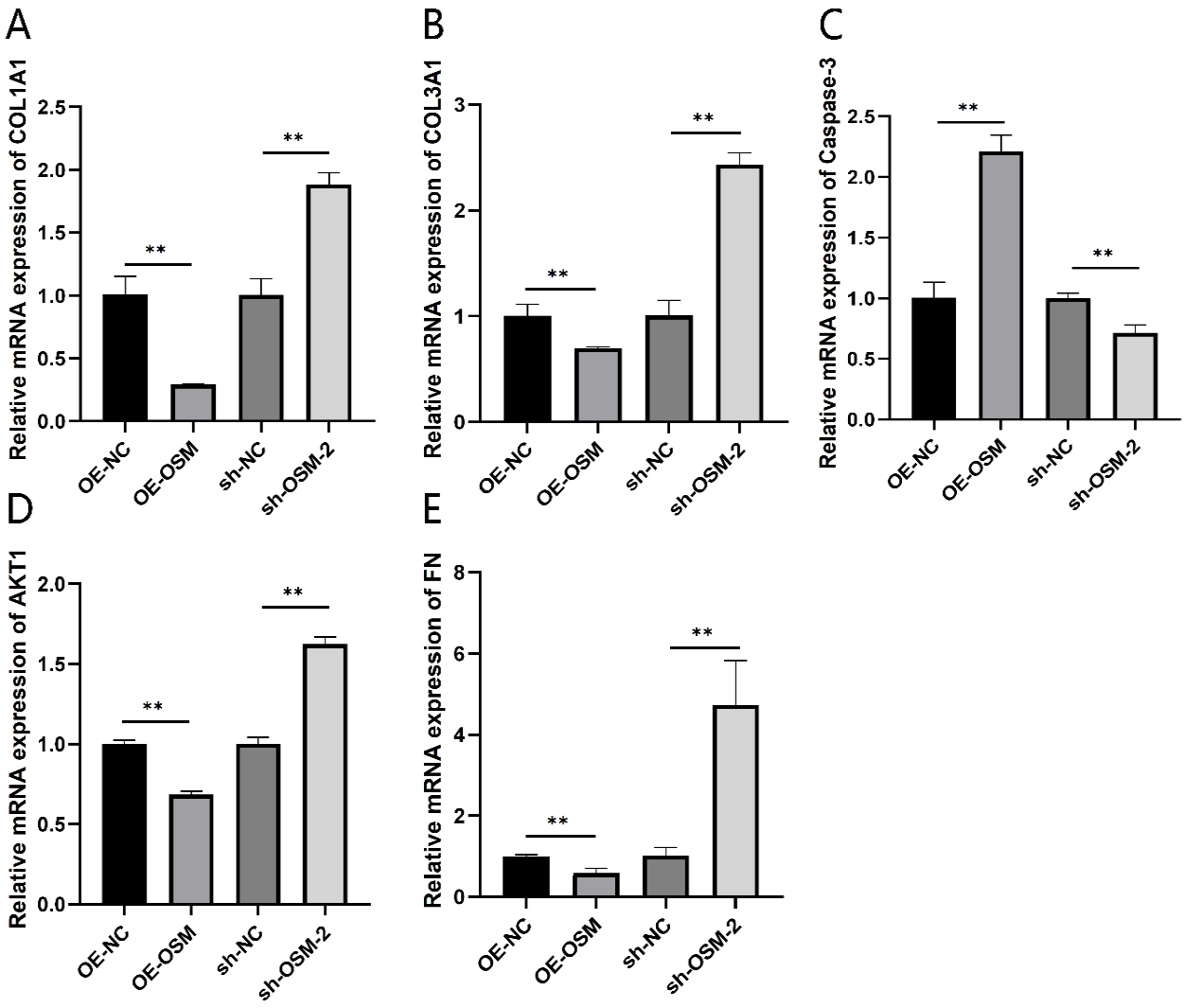

Fig 2: Effects of Overexpression and Interference with *OSM* on mRNA Expression Levels of COL1A1, COL3A1, AKT1, FN and Caspase-3.**P<0.01.A: Expression of COL1A1 (OE-OSM:0.28 ±0.07); B: Expression of COL3A1 (OE-OSM:0.66 ±0.08); C: Expression of Caspass-3 (OE-OSM:2.2 ±0.3); D: Expression of AKT1 (OE-OSM: 0.73 ±0.10); E: Expression of FN (OE-OSM: 0.64 ±0.24). **P<0.01. (n=3 biological replicates per condition).

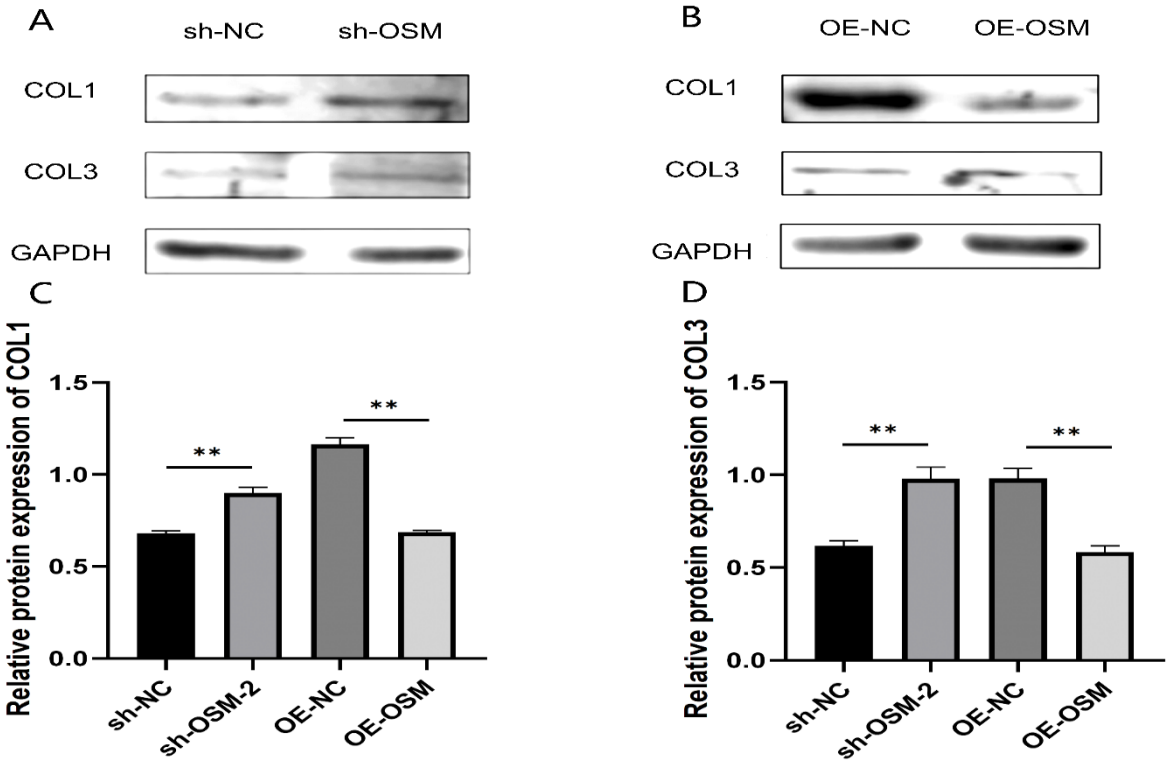

Fig 3: Effect of *OSM* on Key Genes for ECM Deposition. A: Protein expression of COL1 and COL3 was inhibited after OSM; B: Protein expression of COL1 and COL3 was overexpression after OSM; C: Protein expression of COL1 and COL3 was inhibited after OSM (OE-NC: 1.1 ± 0.08; OE-OSM:0.63 ±0.03) **P<0.01; D: Protein expression of COL1 and COL3 was overexpression after OSM (OE-NC: 0.93 ± 0.17; OE-OSM:0.54 ±0.11) **P<0.01.

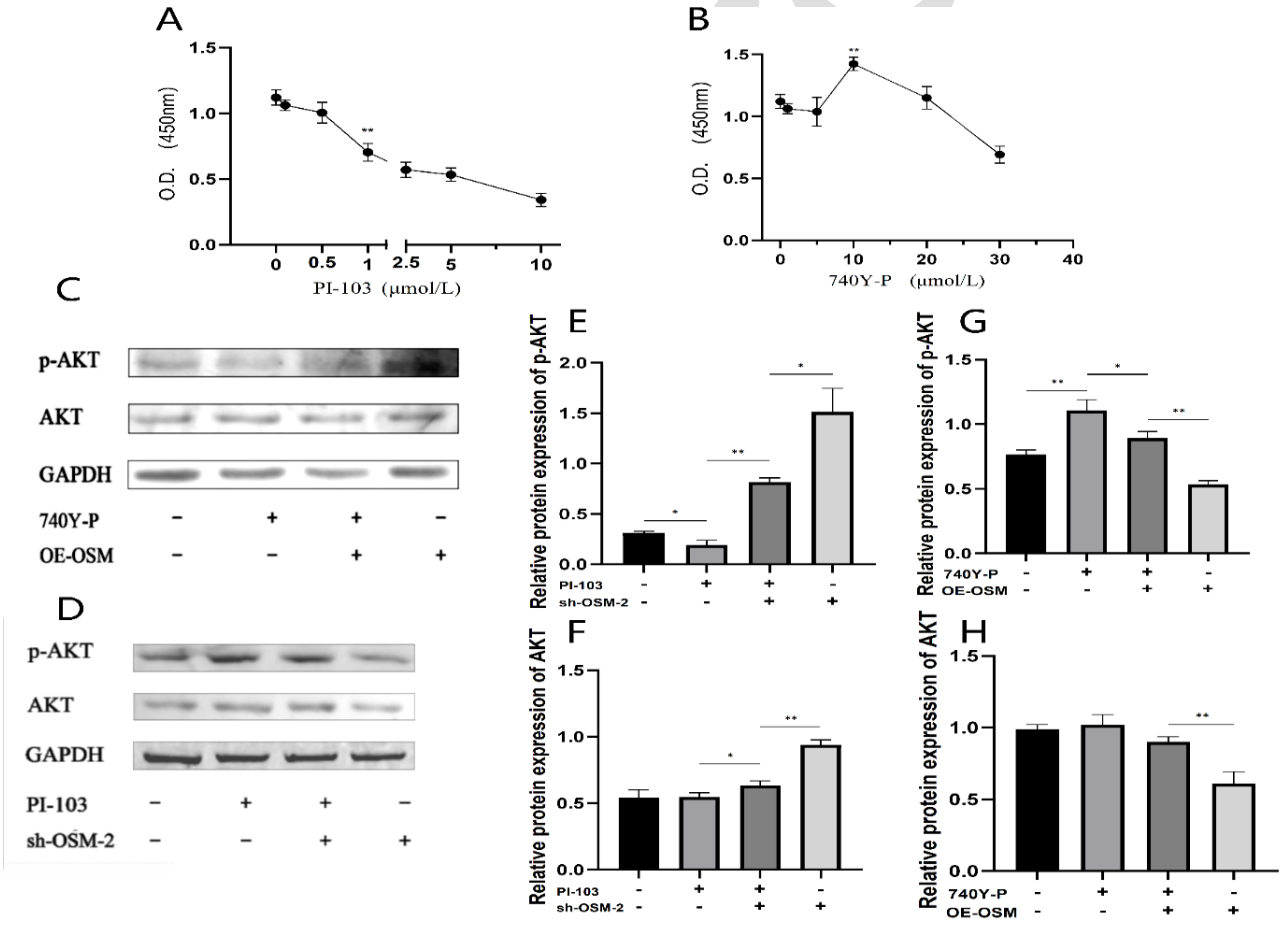

Fig 4: Effect of *OSM* on the PI3K/AKT Pathway. A: Optimal concentration of PI3K agonist (740Y-P); B: Optimal Concentration of PI3K Inhibitor (PI-103); C: Western Blot Assay for AKT; D: Western Blot Assay for p-AKT; E: Effect of pathway inhibitors (PI-103) and OSM inhibition on p-AKT protein expression; F: Effect of pathway inhibitors (PI-103) and OSM inhibition on AKT protein expression; G: Effect of pathway agonist (PI-103) and OSM overexpression on p-AKT protein expression; H:Effect of pathway agonist (PI-103) and OSM overexpression on AKT protein expression. *P<0.05,**P<0.01

concentrations affecting test accuracy, 1μmol/L of PI-103 and 10μmol/L of 740Y-P were chosen for further experiments (Fig. 4). WB assays showed that, compared with the 740Y-P+ and OE-OSM+ group, the p-AKT and AKT expression levels in the OE-OSM+ group were significantly decreased ($P<0.01$). Compared with the 740Y-P- and OE-OSM- group, the p-AKT expression in the 740Y-P+ group significantly increased ($P<0.01$), while the AKT expression showed no significant difference. Compared with the PI-103+ and sh-OSM-2+ groups, the p-AKT and AKT expression levels in the sh-OSM-2+ group were significantly increased ($P<0.05$, $P<0.01$).

DISCUSSION

The results indicated that CCK-8 and plate cloning assays revealed that OSM expression reduced the proliferative capacity of donkey skin fibroblasts, akin to findings by Kan, Cipriano, and Jackson (2011), who observed similar effects in normal mammary epithelial cells treated with OSM. This study employed a scratch assay to simulate the wound healing process, finding that OSM expression markedly inhibited cell migration. These results confirm OSM's suppressive effect on both cell proliferation and migration in donkey skin fibroblasts. However, variations in ligand concentration and cell type suggest that OSM exhibits diverse biological functions in different contexts. However, further studies have revealed that OSM can also exert proliferative effects in various cancer cell lines, such as ovarian (Li *et al.*, 2011) and sarcoma cells (David *et al.*, 2012), while showing contrasting effects in lung epithelial cells, where it stimulates the proliferation of precancerous cells but inhibits that of normal cells (Loewen *et al.*, 2005). Additionally, research by Liu *et al.* (2021), demonstrated that OSM may counteract the inhibitory effects of high glucose on the proliferation and ECM secretion of human skin fibroblasts via the ERK pathway, suggesting that OSM's effects are context dependent. Collectively, these findings emphasize that differences in ligand concentration and cell type contribute significantly to the functional diversity of OSM. The research by Stawski and Trojanowska (2019) has provided some mechanistic explanations for this phenomenon, OSM activates distinct signaling pathways (such as JAK/STAT, MAPK, PI3K/AKT) via two receptor complexes (Type I: LIFRβ/gp130; Type II: OSMRβ/gp130), leading to its dual pro- and anti-fibrotic roles in inflammation, fibrosis, or cancer (Oncostatin M and its role in fibrosis). Further investigation is required to determine the precise conditions under which OSM promotes cell proliferation.

The results indicated that OSM overexpression significantly downregulated the expression of ECM and wound healing-related factors, including COL1A1, COL3A1, FN, and AKT1, at the transcriptional level, while simultaneously increasing the expression of Caspase-3. WB analysis of ECM proteins, specifically collagen types I and III, revealed that OSM inhibited their expression. Conversely, OSM interference induced an increase in collagen expression, suggesting a potential involvement in anti-fibrotic effects within donkey skin fibroblasts. These findings are consistent with those of Vincent Huguier *et al.* (2019). who reported that OSM mitigated TGF-β1-induced expression of fibrosis markers, thus indicating a protective anti-fibrotic effect. Similarly, in a bleomycin-induced pulmonary fibrosis model, transplantation of OSM-pretreated MSCs resulted in improved lung function and reduced levels of inflammatory and fibrotic markers (Lan *et al.*, 2017). OSM reduced collagen 1, collagen 3, and significantly attenuated myocardial tissue fibrosis (Zhu, Xu, and Chen, 2024). These findings suggest OSM generally inhibits ECM deposition, proposing a potential role in scar formation during later wound healing stages.

The PI3K/AKT pathway is crucial for maintaining skin barrier function and is closely associated with tissue regeneration and fibrosis. (Qin *et al.*, 2021). Research indicates that, compared to AKT+/+ mice, AKT-/- mice maintain a healthier alveolar structure, exhibit fewer collagen and ECM components, and have a longer survival time; targeting AKT1 can halt the progression of lung fibrosis (Guo *et al.*, 2023). Our results showed that when overexpressing or interfering with the OSM gene while adding the PI3K/AKT pathway inhibitor PI-103 and the pathway activator 740Y-P, the overexpression of OSM led to decreased expression levels of p-AKT and AKT, and the expression levels increased after applying the corresponding agonist. In contrast, the expression levels of key pathway genes p-AKT and AKT significantly increased after interfering with OSM. These results indicate that OSM can regulate the PI3K/AKT signaling pathway, not only inhibiting AKT activation but also reducing AKT expression by inhibiting the upstream of AKT. It is preliminarily suggested that OSM can affect the proliferation and migration of donkey skin fibroblasts and wound healing-related genes through the PI3K/AKT signaling pathway.

This study has certain limitations. The experiments were only conducted in vitro using normal fibroblasts, without constructing in vivo animal models or pathological fibrosis models. Donkeys have a high infection rate without treatment (Al-Sabaawy and Al-Hyani, 2022). Therefore, the applicability of the research results in actual physiological environments and disease states require further verification. Additionally, the specific mechanism by which OSM exerts its effects through the PI3K/AKT pathway requires further mechanistic investigation.

Future research can be carried out in the following directions. First, establish in vivo animal models of skin fibrosis to validate the role and mechanism of OSM in vivo. Second, use pathological fibrosis models to clarify the regulatory effect of OSM on fibroblasts in disease states. Finally, conduct in-depth research on the upstream and downstream molecular mechanisms of the PI3K/AKT pathway to more comprehensively reveal the action pathway of OSM, which provides possibilities for the treatment of skin wound healing and fibrosis diseases.

Conclusions: This study demonstrates that OSM significantly inhibits the proliferation and migration of donkey skin fibroblasts, downregulates ECM gene expression, and modulates the PI3K/AKT signaling pathway. These results offer novel insights into the regulatory role of OSM in fibroblast activity during skin wound healing and underscore its therapeutic potential for controlling fibrous scar formation. Although these findings are based on in vitro experiments, further validation

through in vivo studies using relevant animal models is required to substantiate the antifibrotic efficacy of OSM and support its clinical application in the management of fibrotic diseases.

Acknowledgments: This research was funded by the Science and Technology Plan Projects of Ili Kazakh Autonomous Prefecture, Xinjiang (YXC2023A07) and Science and Technology Programme Projects in Keke Dara City, Fourth Division (2024GG019)

Conflicts of Interest: The authors declare no conflicts of interest.

Author Contributions: Conceptualization, LL, YZ, RS, CW, and HT; methodology, LL, YZ, TZ and HT; validation, YZ and RS, formal analysis, LL and CZ; investigation, LL and CZ; data curation, CZ; writing - original Draft, CZ; writing - review & editing, LL; visualization, LL and CZ; supervision, LL, MG, WZ and YW; project administration, LL, YZ, RS, and TH; funding acquisition, MG; All authors have read and agreed to the published version of the manuscript.

REFERENCES

Al-Sabaawy DM and Al-Hyani O, 2022. Effect of Aloe vera gel on the healing of cutaneous wounds in donkeys. IJVS 36:425–432.

Anantama NA, Du Cheyne C, Martens A, *et al*., 2022. The granulation (t)issue: A narrative and scoping review of basic and clinical research of the equine distal limb exuberant wound healing disorder. Vet J 280:105790.

Azari O, Molaei MM and Hojabri R, 2012. Differences in second-intention wound healing of distal aspect of the limb between Caspian miniature horses and donkeys: macroscopical aspects. Comp Clin Pathol 21:731–735.

Caligiuri A, Gitto S, Lori G, *et al*., 2022. Oncostatin M: From Intracellular Signaling to Therapeutic Targets in Liver Cancer. Cancers 14:4211.

Carsuzaa F, Béquignon É, Bainaud M, *et al*., 2022. Oncostatin M Counteracts the Fibrotic Effects of TGF-β1 and IL-4 on Nasal-Polyp-Derived Fibroblasts: A Control of Fibrosis in Chronic Rhinosinusitis with Nasal Polyps? IJMS 23:6308.

David E, Tirode F, Baud'huin M, *et al*., 2012. Oncostatin M Is a Growth Factor for Ewing Sarcoma. Am J Pathol 181:1782–1795.

Gardeazabal L and Izeta A, 2024. Elastin and collagen fibres in cutaneous wound healing. Exp Dermatol 33:e15052.

Graupera M, Guillermet-Guibert J, Foukas LC, *et al*., 2008. Angiogenesis selectively requires the p110α isoform of PI3K to control endothelial cell migration. Nature 453:662–666.

Guo C, Liang L, Zheng J, *et al*., 2023. UCHL1 aggravates skin fibrosis through an IGF -1-induced Akt/ mTOR / HIF -1α pathway in keloid. FASEB J 37:e23015.

Han N-R, Ko S-G, Park H-J, *et al*., 2021. Dexamethasone Attenuates Oncostatin M Production via Suppressing of PI3K/Akt/NF-κB Signaling in Neutrophil-like Differentiated HL-60 Cells. Molecules 27:129.

Hao Z, Huajun S, Zhen G, *et al*., 2023. AQP8 promotes glioma proliferation and growth, possibly through the ROS/PTEN/AKT signaling pathway. BMC Cancer 23:516.

He J, Fang B, Shan S, *et al*., 2024. Mechanical stiffness promotes skin fibrosis through FAPα-AKT signaling pathway. J Dermatol Sci 113:51–61.

He Q, Jia L, Wang X, *et al*., 2023. Knockdown of BUB1 inhibits tumor necrosis factor-α-induced proliferation and migration of rheumatoid arthritis synovial fibroblasts by regulating PI3K /Akt pathway. Int J of Rheum Dis 26:2024–2030.

Huang Y, Zhao H, Zhang Y, *et al*., 2023. Enhancement of Zyxin Promotes Skin Fibrosis by Regulating FAK/PI3K/AKT and TGF-β Signaling Pathways via Integrins. Int J Biol Sci 19:2394–2408.

Huguier V, Giot J-P, Simonneau M, *et al*., 2019. Oncostatin M exerts a protective effect against excessive scarring by counteracting the inductive effect of TGFβ1 on fibrosis markers. Sci Rep 9:2113.

Iacopetti I, Patruno M, Melotti L, *et al*., 2020. Autologous Platelet-Rich Plasma Enhances the Healing of Large Cutaneous Wounds in Dogs. Front Vet Sci 7:575449.

Jørgensen E, Hjerpe FB, Hougen HP, *et al*., 2020. Histologic changes and gene expression patterns in biopsy specimens from bacteria-inoculated and noninoculated excisional body and limb wounds in horses healing by second intention. Ajvr 81:276–284.

Johnson BZ, Stevenson AW, Prêle CM, *et al*., 2020. The Role of IL-6 in Skin Fibrosis and Cutaneous Wound Healing. Biomedicines 8:101.

Kan CE, Cipriano R and Jackson MW, 2011. c-MYC Functions as a Molecular Switch to Alter the Response of Human Mammary Epithelial Cells to Oncostatin M. Cancer Res 71:6930–6939.

Knottenbelt DC, 2019. Skin Disorders of the Donkey and Mule. Vet Clin North Am Equine Pract 35:493–514.

Lan Y-W, Theng S-M, Huang T-T, *et al*., 2017. Oncostatin M-Preconditioned Mesenchymal Stem Cells Alleviate Bleomycin-Induced Pulmonary Fibrosis Through Paracrine Effects of the Hepatocyte Growth Factor. Stem Cells Transl Med 6:1006–1017.

Li Q, Zhu J, Sun F, *et al*., 2011. Oncostatin M promotes proliferation of ovarian cancer cells through signal transducer and activator of transcription 3. Int J Mol Med 28:101–108.

Liu L, Fu X, Xue B, *et al*., 2021. Effect of oncostatin M on proliferation and secretion of extracellular matrix in human dermal fibroblasts in high glucose condition. J Third Mil Med 43:955–963.

Loewen GM, Tracy E, Blanchard F, *et al*., 2005. Transformation of human bronchial epithelial cells alters responsiveness to inflammatory cytokines. BMC Cancer 5:145.

Mashimo K, Usui-Ouchi A, Ito Y, *et al*., 2021. Role of oncostatin M in the pathogenesis of vernal keratoconjunctivitis: focus on tissue remodeling. Jpn J Ophthalmol 65:144–153.

Mohammed ESI, Madkour FA, Zayed M, *et al*., 2022. Comparative histological analysis of the skin for forensic investigation of some animal species. EXCLI J; 21:Doc1286; ISSN 1611-2156.

Peña OA and Martin P, 2024. Cellular and molecular mechanisms of skin wound healing. Nat Rev Mol Cell Biol 25:599–616.

Polak KL, Tamagno I, Parameswaran N, *et al*., 2023. Oncostatin-M and OSM-Receptor Feed-Forward Activation of MAPK Induces Separable Stem-like and Mesenchymal Programs. Mol Cancer Res 21:975–990.

Polidori P, Vincenzetti S, Pucciarelli S, *et al*., 2020. Comparison of Carcass and Meat Quality Obtained from Mule and Donkey. Animals 10:1620.

Qin W, Cao L and Massey IY, 2021. Role of PI3K/Akt signaling pathway in cardiac fibrosis. Mol Cell Biochem 476:4045–4059.

Richards CD, 2013. The Enigmatic Cytokine Oncostatin M and Roles in Disease. ISRN Inflamm 2013:1–23.

Seaton M, Hocking A and Gibran NS, 2015. Porcine Models of Cutaneous Wound Healing. ILAR J 56:127–138.

Sood RF, Muffley LA, Seaton ME, *et al*., 2015. Dermal Fibroblasts from the Red Duroc Pig Have an Inherently Fibrogenic Phenotype: An In Vitro Model of Fibroproliferative Scarring. Plast Reconstr Surg 136:990–1000.

Stawski L and Trojanowska M, 2019. Oncostatin M and its role in fibrosis. Connect Tissue Res 60:40–49.

Tracy LE, Minasian RA and Caterson EJ, 2016. Extracellular Matrix and Dermal Fibroblast Function in the Healing Wound. Adv Wound Care 5:119–136.

Wei S, Chen Y, Shi X, *et al*., 2023. OSM May Serve as a Biomarker of Poor Prognosis in Clear Cell Renal Cell Carcinoma and Promote Tumor Cell Invasion and Migration. Int J Genomics 2023:1–15.

Zhu C, Wang Y, Zhao Y, *et al*., 2023. Primary culture and identification of the fibroblasts of Xinjiang donkeys. Heilongjiang Anim Sci Vet Med 113-116+121+132.

Zhu Y, Hu X, Zhang J, *et al*., 2020. Extracellular Vesicles Derived From Human Adipose-Derived Stem Cell Prevent the Formation of Hypertrophic Scar in a Rabbit Model. Ann Plast Surg 84:602–607.

Zhu Y, Xu Z and Chen M, 2024. Study on the mechanism of OSM participating in myocardial fibrosis by inhibiting TGFβ-induced EndMT of cardiac microvascular endothelial cells through SPARC/SMAD signaling. Naunyn Schmiedebergs Arch Pharmacol 398:4479–4489.